Visible photoluminescence from Er^{3+} ions in *a*-SiN alloys

A. R. Zanatta, M. J. V. Bell, and L. A. O. Nunes
Instituto de Física de São Carlos, Universidade de São Paulo, P.O. Box 369, São Carlos, S.P., 13560-970, Brazil
(Received 30 October 1998)

Thin films of Er-doped amorphous SiN (*a*-SiErN) alloys have been prepared by cosputtering under different deposition conditions. Infrared absorption, Raman scattering, and photoluminescence spectroscopy were employed for characterization purposes. The strongest Er^{3+}-related emissions in the *a*-SiErN films take place at ~525, 550, and 1540 nm, corresponding to the $^2H_{11/2}\rightarrow{}^4I_{15/2}$, $^4S_{3/2}\rightarrow{}^4I_{15/2}$, and $^4I_{13/2}\rightarrow{}^4I_{15/2}$ transitions, respectively. Sample characterization pointed out interesting features following the photon excitation energy, Er concentration, and thermal anneals which are directly related to the electronic structure of the *a*-SiErN films. Based on these experimental data some mechanisms associated with the Er^{3+}-ion excitation and recombination are proposed and discussed in detail. The present study demonstrates that Er^{3+} ions in combination with the wide-band-gap *a*-SiN semiconductor allow the achievement of very narrow green light emission at room temperature. In addition to the potential applications of SiEr-based compounds in the infrared energy region (light sources, detectors, optical amplifiers, etc.), the present results enlarge the perspectives of their use in the construction of monochromatic large-area flat-panel displays, visible light-emitting diodes, temperature sensors, etc. [S0163-1829(99)04915-2]

I. INTRODUCTION

Since the early ages of the (micro)electronics industry, Si has played a fundamental and decisive role in modern life. Its dominance over other semiconductors is a direct consequence of its superior material and processing properties as well as to its mature technology.[1] Taking into account its natural abundance and chemical simplicity, another semiconductor is not likely to displace Si as the material of choice in current electronic applications. Notwithstanding some clear advantages, Si is known to be a very poor light emitter, avoiding its large use in optical applications. However, the realization of an all Si-based hybrid optoelectronic device is so appealing that innumerous efforts have been made in order to improve optical activity in silicon.[2] Toward this end, besides the engineering of low-dimensional structures, the doping of Si with luminescent centers like rare-earth ions, for example, deserves special attention.[2–4] Rare-earth (RE) doping of Si systems has been the subject of intensive research throughout the past years because of the systems' potential to combine sharp, temperature-stable RE luminescence with the convenience of electrical excitation via the semiconductor host.[5] Erbium-doped materials, in particular, are of great interest since the $^4I_{13/2}\rightarrow{}^4I_{15/2}$ transition of Er^{3+} ions at ~1540 nm matches the minimum loss region of the current silica fibers used in optical communications.[6] Progress toward practical devices based on these compounds, however, has been hindered in part by their low room-temperature efficiency.[7] As a consequence, any improvement in the performance of these devices would rely, necessarily, on a better understanding of the nature of RE centers in different hosts,[8–10] as well as on the basic mechanisms of RE excitation.[11]

Most of the current efforts in the field of Er-doped compounds are concerned just with the infrared emission at ~1540 nm.[5] Er^{3+} ions, however, are known to exhibit radiative transitions at different wavelengths spanning the almost entire electromagnetic spectrum.[12] As a consequence, visible light emission due to Er^{3+} are expected to occur in wide-band-gap materials. Despite the relatively large band gap of some of the most studied Er-doped semiconductors, Er^{3+}-related visible emissions were verified only from SiO,[9] SiN,[10] and GaN (Ref. 13) compounds. The absence of visible Er^{3+}-related emission from certain wide-band-gap compounds can be related either to electronic or structural characteristics, for example, and clearly deserves more study. (The lack of reports in this field could also be a mere reflex of no specific investigations.) In addition to electronic and structural aspects, the energy of optical excitation plays a crucial role in achieving visible Er^{3+}-related emission in different hosts. Figure 1, for example, shows a photoluminescence (PL) spectra of one Er-doped *a*-SiN alloy at 6 K under different photon excitation energies. According to Fig. 1, a very broad signal due to the *a* matrix is present in all curves, their maximum intensities being dependent on the excitation energy.[14,15] Emission due to Er^{3+} is verified just under optical pumping with photons of 488.0 nm which resonantly populates its $^4F_{7/2}$ energy level.[10,12] Regardless of the semiconducting host and its peculiarities, the achievement of commercially attractive Er-doped devices should be (in some way) compatible with the existing Si technology. As a consequence, both the growth method and the processing temperatures must be a matter of concern. In this respect, the present paper deals with a systematic study of *a*-SiErN films. Based on the optical spectroscopic characterization of this SiEr system, its main features are presented and discussed.

II. EXPERIMENTAL DETAILS

All *a*-SiErN thin films were prepared by the radio-frequency (13.56 MHz) reactive sputtering method according to different deposition conditions in a high vacuum system. During deposition, a 99.999% Si target partially covered at random with metallic 99.9% Er platelets and ultrahigh-purity

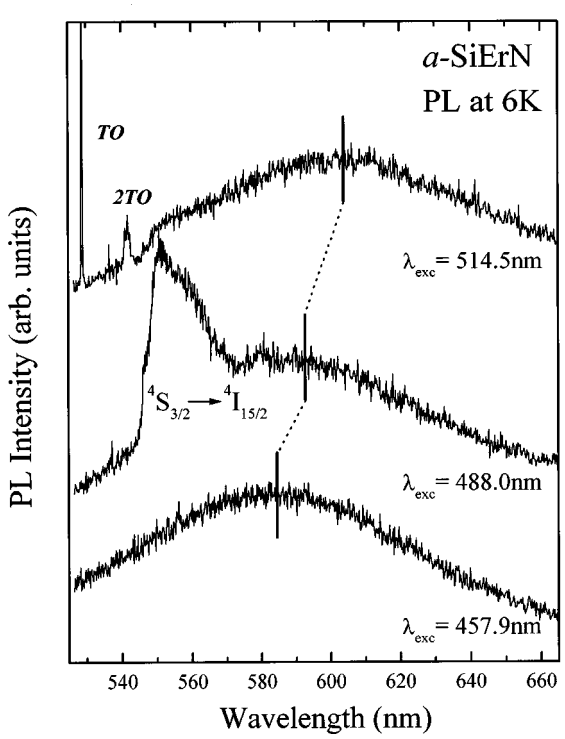

FIG. 1. Photoluminescence (PL) intensity in the ~530–660-nm wavelength range of one *a*-SiErN thin film. The spectra were taken at 6 K under different photon excitation energies. The spectra have been vertically shifted for clarity. TO and 2TO stand for the transverse optical phonons of first and second order due to the *c*-Si substrate, respectively. A very broad light emission from the amorphous matrix (identified with small vertical bars) can be observed in the ~580–600-nm region, depending on the photon excitation. Under 488-nm optical pumping the $^4S_{3/2} \rightarrow {}^4I_{15/2}$ transition characteristic of Er^{3+} ions is also observed.

($[H_2O] < 3$ ppm) gases were employed. Polished *p*-type crystalline (*c*-)Si wafers and quartz plates were used as substrates in every deposition run. Substrate temperature (T_s), total pressure (P_T), N_2 to Ar partial pressure ratio (R), and target voltage bias (V_b) were within the adopted deposition parameters and are displayed in Table I. For the whole *a*-SiErN sample series, the Er concentration was modified according to the relative Er to Si target area. In addition to Ar and N_2, sample *B* was deposited with a partial pressure of 0.4 mTorr of H_2. A nonintentionally hydrogenated Er-free *a*-SiN host (sample *E*) was also deposited for comparison purposes.

TABLE I. Deposition conditions adopted in the series of *a*-Si(Er)N samples. The following parameters were varied: T_s (substrate temperature), P_T (total pressure), R (N_2/Ar partial pressure ratio), V_b (target bias voltage), P (rf power density), t_d (time of deposition), and Er/Si (relative Er/Si target area). RT stands for room temperature. Sample *B* corresponds to an intentionally hydrogenated thin film.

Sample	T_s (°C)	P_T (mTorr)	R	V_b (kV)	P (W cm^{-2})	t_d (min)	Er/Si
A	200	10	1	0.7	~2	180	~0.1
B	RT	1	0.1	1.2	~0.85	360	~0.03
C	RT	1	0.5	1.2	~0.85	480	~0.03
D	RT	1	0.5	1.2	~0.85	360	~0.06
E	RT	1	0.5	1.2	~0.85	300	0

Typical sample characterization included (a) PL measurements as a function of photon excitation energy and temperature of measurement, both in the infrared (IR) and visible (VIS) energy ranges; (b) IR transmission in the 400–6000-cm^{-1} wave-number range; (c) Raman scattering; and (d) optical absorption in the UV-VIS energy region. The sample thickness and index of refraction were achieved from the interference fringes present in the UV-VIS spectra.[16] The E_{03} and E_{04} optical gaps (the energy at which the absorption coefficient reaches 10^3 and 10^4 cm^{-1}) were also derived from the UV-VIS curves. After measurement, the IR spectra were conveniently processed[17] in order to obtain the various absorption bands (and corresponding concentration)[18] of light atoms bonded to Si.

III. RESULTS

The following refers to two main classes of results called *as-deposited* (without any kind of treatment) and *thermal-annealed* samples (submitted to isochronal thermal treatments).

As-deposited *a*-SiErN samples

Valuable insights into the chemical bonding of *a* films can be gained from IR spectroscopy. Figure 2 shows the IR-absorption spectra of all studied samples. According to the experimental data, at least seven absorption bands could be observed, and were identified as follows:[19,20] band 1 (~480 cm^{-1}), due to the Si-Si breathing mode; band 2 (~640 cm^{-1}), due to the Si-H bending mode; band 3 (~880 cm^{-1}), due to the Si-N asymmetric stretching mode; band 4 (~1060 cm^{-1}), due to the Si-O stretching mode; band 5 (~1175 cm^{-1}), due to the N-H bending mode; band 6 (~2200 cm^{-1}), due to the Si-H stretching mode; and band 7 (~3350 cm^{-1}), due to the N-H stretching mode. Notice that, without exception, all *a*-Si(Er)N films present hydrogen and oxygen atoms in their matrices, most probably, as a consequence of the residual H_2O in the gaseous sources employed. The superficial oxidation of the Er platelets can also contribute to the presence of oxygen in the *a*-SiErN films. Still related to Fig. 2 and Table I, a high-power density (or intentional H_2) during deposition greatly improve the number of Si-H (or N-H) species. In order to determine the composition of each different sample the integrated absorption of bands 2, 3, 4, and 7 were used to estimate the concentration of Si-H, Si-N, Si-O, and N-H species, respectively. A summary of these compositional information as well as some optical data of the *a*-Si(Er)N sample series can be found in Table II.

According to the literature, crystalline or ordered Si_3N_4-based compounds are expected to present narrow Raman features mainly at[21] ~450, 630, 740, 865, and 920 cm^{-1}. In this sense, the morphology of the as-deposited *a*-Si(Er)N thin films were investigated by means of Raman-scattering spectroscopy (Fig. 3). All Raman spectra were taken from films deposited on *c*-Si substrates by exciting with 514.5-nm photons. As a consequence, and taking into

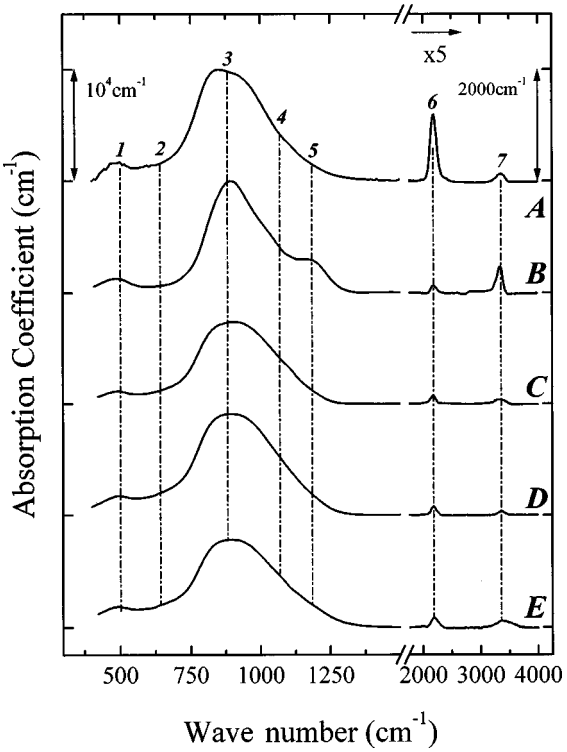

FIG. 2. Infrared-absorption features of the series of *a*-Si(Er)N samples. The spectra have been vertically shifted for clarity. Note the multiplying factor in the ~2000–4000-cm^{-1} region. The main absorption bands were identified with numbers and correspond to the following: band 1—Si-Si breathing mode; band 2—Si-H bending mode; band 3—Si-N asymmetric stretching mode; band 4—Si-O stretching mode; band 5—N-H bending mode; band 6—Si-H stretching mode; band 7—N-H stretching mode.

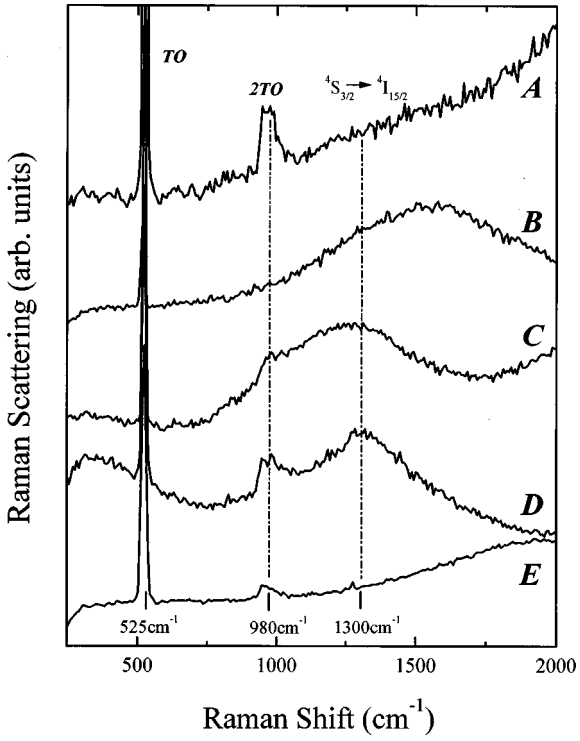

FIG. 3. Room-temperature Raman-scattering spectra of the as-deposited *a*-Si(Er)N samples under excitation with 514.5-nm photons. The curves have been vertically shifted for clarity. The signals at ~525, 980 (and 1300 cm^{-1}) correspond to the *c*-Si transverse optical of first TO and second-order 2TO phonons (and to the $^4S_{3/2} \rightarrow {}^4I_{15/2}$ green Er^{3+} transition), respectively. Also present in the figure, the broader and stronger signals are due to the PL of the *a*-SiN matrix.

account the optical gap of these compounds (see Table II), the transverse optical of first (TO) and second-order (2TO) phonons of the *c*-Si substrates were observed at ~525 and 980 cm^{-1}, respectively.[22] Raman measurements of films deposited on quartz substrates have also been performed, and do not present scattered light at ~525 and 980 cm^{-1}. In addition to the TO and 2TO signals, Fig. 3 also displays the PL from the *a*-SiN matrix. At this point, it is noteworthy to mention that interference fringes due to the film-substrate interface will also be evident from the PL spectra. These interference fringes are at the origin of the different maxima observed in Fig. 3, and correspond to the PL of the *a*-SiN matrix. Sample *D* in Fig. 3 also exhibits a faint signal at ~1300 cm^{-1} which is due to the $^4S_{3/2} \rightarrow {}^4I_{15/2}$ green Er^{3+}-related transition.[10]

PL measurements have been carried out under different pumping wavelengths from an Ar^+ laser (363.8, 457.9, 476.5, 488.0, and 514.5 nm). From our previous efforts,[10]

TABLE II. Optical and compositional data of the *a*-Si(Er)N samples. Sample thickness (*d*) and refractive index (*n*) were achieved from the UV-VIS transmission curves. The E_{03} and E_{04} optical gaps (energy at which the absorption coefficient reaches 10^3 and 10^4 cm^{-1}, respectively) were also obtained from the UV-VIS spectra. The concentration of Si-H (at 2200 cm^{-1}), Si-N (at 880 cm^{-1}), Si-O (at 1060 cm^{-1}), and N-H (3350 cm^{-1}) species were estimated by using their integrated areas and respective calibration constants ($k_{\text{Si-H}} = 2.2\times10^{20}$ cm^{-2}, $k_{\text{Si-N}} = 5.0\times10^{18}$ cm^{-2}, $k_{\text{Si-O}} = 2.5\times10^{18}$ cm^{-2}, and $k_{\text{N-H}} = 2.8\times10^{20}$ cm^{-2}). na means not available.

Sample	*d* (μm)	*n* @500 nm	E_{04} (eV)	E_{03} (eV)	Si-H (cm^{-3})	Si-N (cm^{-3})	Si-O (cm^{-3})	N-H (cm^{-3})
A	0.5	na	na	na	1.6×10^{22}	1.8×10^{22}	3.0×10^{19}	1.8×10^{21}
B	3.1	1.72	5.4	4.5	2.0×10^{21}	1.2×10^{22}	2.5×10^{21}	1.1×10^{22}
C	4.7	1.75	4.9	3.9	2.6×10^{21}	1.2×10^{22}	8.5×10^{20}	1.2×10^{21}
D	3.6	1.77	5.1	3.9	2.2×10^{21}	1.7×10^{22}	7.0×10^{20}	1.4×10^{21}
E	3.3	1.79	5.0	3.7	1.8×10^{21}	1.5×10^{22}	3.5×10^{20}	1.5×10^{21}

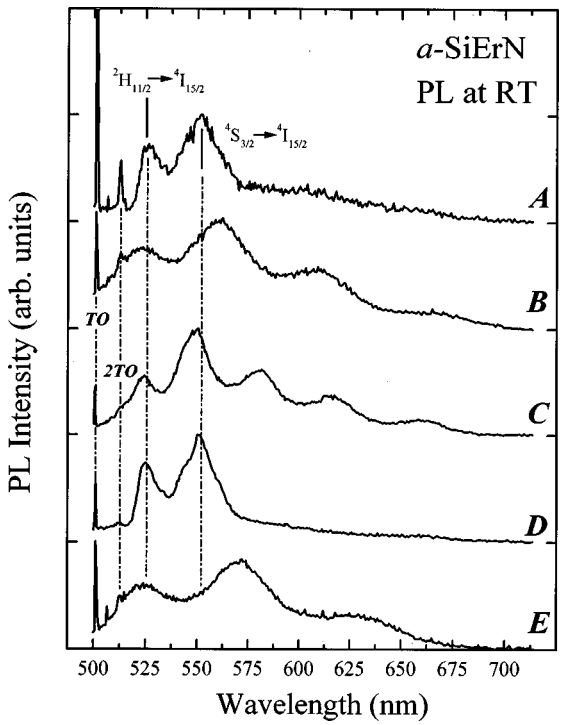

FIG. 4. Room-temperature PL intensity under 488.0-nm photon excitation for the whole *a*-Si(Er)N sample series. All spectra have been normalized and vertically shifted for clarity. The TO and 2TO Raman-scattered light (at ~500.9 and 512.6 nm) due to the *c*-Si substrate are evident in all spectra. Note, however, their relative intensities with the PL signals at ~550 nm. Light emission from the *a*-SiN matrix can also be observed with their respective interference fringes in samples *B*, *C*, and *E*. The PL due to the Er^{3+} ions ($^2H_{11/2}\rightarrow{}^4I_{15/2}$ and $^4S_{3/2}\rightarrow{}^4I_{15/2}$ transitions at ~525 and 550 nm, respectively) can be clearly observed from samples *A* and *D*.

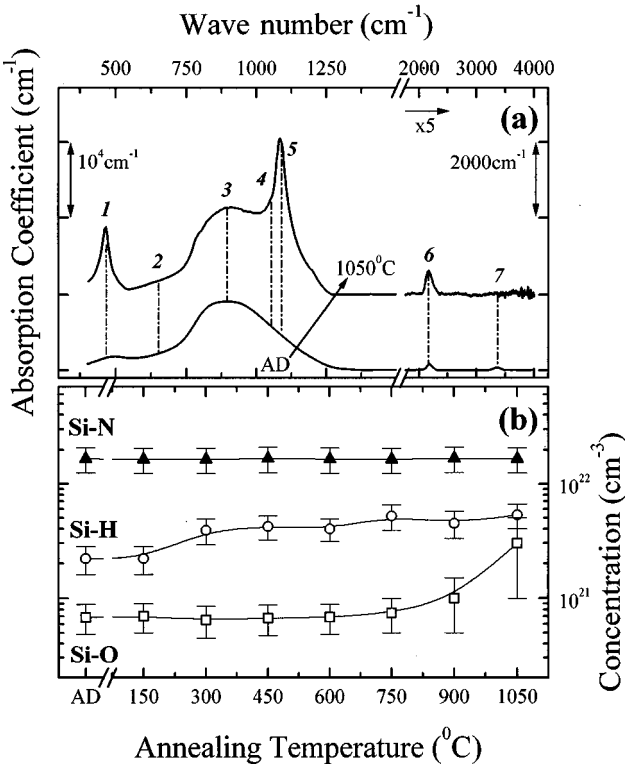

FIG. 5. Infrared-absorption data of one *a*-SiErN thin film (sample *D*) according to different thermal treatments. (a) presents the absorption bands relative to the as-deposited (AD) and thermal-annealed (1050 °C) *a*-SiErN films. The absorption bands indicated with numbers correspond to those identified in Fig. 2. Note the multiplying factor used in the ~2000–4000-cm^{-1} region. (b) displays the estimated concentration of Si-H, Si-N, and Si-O species, as determined from the IR-absorption analysis, according to the different thermal anneals.

and as can be seen from Fig. 1, the most convenient way to extract green Er^{3+}PL from the *a*-SiErN samples is with 488.0-nm photon excitation that resonantly populates the $^4F_{7/2}$ energy levels of the Er^{3+} ions.[10,12] Figure 4 displays the room-temperature PL spectra of the *a*-Si(Er)N samples under excitation with 488.0-nm photons. According to these spectra, the Raman signal due to the *c*-Si substrate (TO and 2TO) and the PL coming from the *a* matrix (with their respective interference fringes) are evident. Moreover, two other features at ~525 and 550 nm are apparent from Fig. 4, and correspond to the $^2H_{11/2}\rightarrow{}^4I_{15/2}$ and $^4S_{3/2}\rightarrow{}^4I_{15/2}$ transitions, respectively.[12]

In view of the above experimental results, some partial conclusions can be drawn: (a) Despite their quite different deposition conditions, all the *a*-Si(Er)N samples considered in this study presented similar compositional and structural characteristics (Figs. 2 and 3). While a high-power density during deposition increases the concentration of Si-H species, the intentional use of hydrogen does not cause appreciable changes in the PL of the *a*-SiN matrix (Fig. 4). (b) There is no evidence of structural order in all the studied *a*-Si(Er)N films. This can be seen either from the Raman spectra (Fig. 3) or based on the linewidth[15] of the PL signal due to the SiN matrix (Fig. 4). (c) A nonintentionally hydrogenated *a*-SiN matrix with a high Er content (Table I)[23] proved to be one of the best for an efficient green emission due to the Er^{3+} ions (Fig. 4). It is believed that a high number of Er^{3+} ions improves the optical absorption of 488.0 nm photons which, in association with the absence of hydrogen atoms, partially inhibits the PL of the *a*-matrix.[10] Based on this evidence, the next step was the investigation of thermal treatments (150–1050 °C range) on the properties of sample *D*.

Thermal annealed *a*-SiErN sample

The isochronal thermal anneals (15 min each) were cumulative, and performed in a temperature-controlled furnace at atmospheric pressure. Figure 5 shows the main results from the IR-absorption analysis. Figure 5(a) illustrates the absorption curves of sample *D*: as deposited and thermal annealed (TA) at 1050 °C. Since all the TA samples were done under noncontrolled conditions (atmospheric pressure) some surface oxidation is expected and indeed verified at high temperatures (band 5). This surface oxidation is also at the origin of the increased absorption at ~480 cm^{-1} (band 1). The increase in the number of Si-H species (band 6) can be associated with either the hydrogen diffusion (mainly from the N-H bonds) or as a consequence of the anneals at atmospheric pressure. Finally, Fig. 5(b) shows the estimated concentration of Si-H, Si-N, and Si-O species as determined from their respective absorption bands.

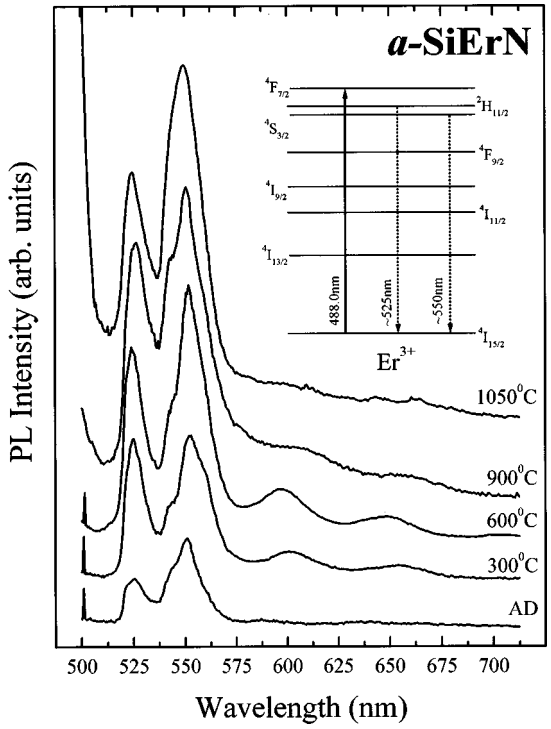

FIG. 6. Photoluminescence intensity (at room temperature) of sample *D* excited with 488.0-nm photons, according to different thermal treatments. The main signals at ~525 and 550 nm are attributed to the $^2H_{11/2}\rightarrow{}^4I_{15/2}$ and $^4S_{3/2}\rightarrow{}^4I_{15/2}Er^{3+}$ transitions, respectively. The peaks at ~600 and 650 nm correspond to interference fringes of the *a*-SiN matrix PL. The inset contains a diagram of the energy levels of an Er^{3+} ion. The thick upward and the dotted downward arrows correspond to photon excitation and Er^{3+}-related PL emission, respectively.

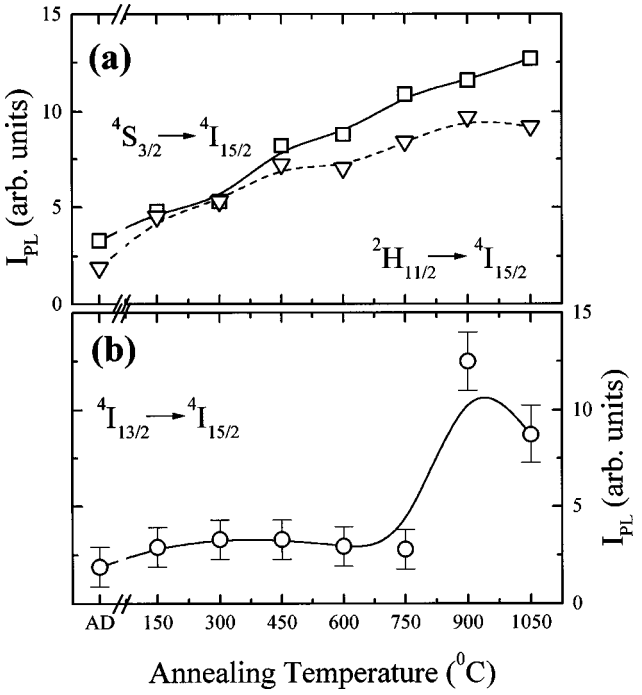

FIG. 7. Photoluminescence intensity (I_{PL}) as a function of annealing temperature. (a) I_{PL} of the $^4S_{3/2}\rightarrow{}^4I_{15/2}$ and $^2H_{11/2}\rightarrow{}^4I_{15/2}$ transitions at ~525 and 550 nm, respectively. (b) I_{PL} corresponding to the $^4I_{13/2}\rightarrow{}^4I_{15/2}$ transition at ~1540 nm. The lines joining the experimental points are just guides to the eyes. AD stands for as-deposited samples.

Raman-scattering spectroscopy was performed in sample *D* after each thermal anneal, revealing no structural changes and/or the appearance of any ordered SiN structure, even after treatments at 1050 °C.[24] The optical band gap of the *a*-SiErN films was also investigated as a function of the different thermal anneals. No significant change could be observed, and the E_{03} band gap remained around 4.0 $\pm$0.5 eV.

PL measurements, by the other hand, presented the most interesting results, which are displayed in Fig. 6. According to Fig. 6 the main features are due to the $^2H_{11/2}\rightarrow{}^4I_{15/2}$ (at ~525 nm) and $^4S_{3/2}\rightarrow{}^4I_{15/2}$ (at ~550 nm) Er^{3+} transitions (see the inset of Fig. 6), and an overall increase in the PL intensity can be observed as the sample is submitted to anneals at higher temperatures. Besides the improvement in the Er^{3+}-related PL intensity, emission from the *a*-SiN matrix can also be observed after anneals at temperatures higher than 300 °C. At 1050 °C the interference fringes are partially destroyed due to an increased surface roughness.[25]

IV. DISCUSSION

The precise role played by thermal anneals in different Er-doped semiconductors (either amorphous or crystalline) still remains a matter of debate. Among the various propositions, thermal treatments on these compounds have been usually associated with[26,27] irradiation damage anneal due to the Er (and/or impurities) implantation, Er (and/or impurities) diffusion, optical activation of Er^{3+} centers, etc. Since the current samples have been prepared by cosputtering, it is believed that thermal anneals can promote some structural rearrangement in the *a*-SiN network even if not detectable by Raman spectroscopy.[24,25] The diffusion of atomic species like hydrogen, nitrogen, and oxygen should also be considered to act in order to passivate dangling bonds.[28] In other words, the PL enhancement, both of the Er^{3+} ions and of the *a*-SiN matrix, must be directly associated with the suppression of nonradiative centers. The nonintentional oxidation of the annealed *a*-SiErN films can also contribute to the increased PL of the Er^{3+} ions, giving rise to a more ionic chemical environment.[29] It is important to note, however, that not only light emission in the VIS energy region has been improved with thermal anneals. The same was also verified for the $^4I_{13/2}\rightarrow{}^4I_{15/2}$ Er^{3+} transition at ~1540 nm.

The overall influence of each thermal anneal on the Er^{3+}-related PL intensities at ~525, 550, and 1540 nm is represented in Fig. 7. According to the figure a clear increase in the PL at ~525 and 550 nm can be observed for all thermal treatments [Fig. 7(a)]. Light emission in the IR (~1540 nm), on the other hand, exhibits a comparable improvement only after treatments at temperatures higher than ~750 °C [Fig. 7(b)]. A possible reason for such a behavior could be associated with the nonintentional augmented number of Si-O species (see Fig. 5). Moreover, taking into account that no appreciable changes have occurred in the band gap of these films, the optical pumping of the $^4F_{7/2}$ Er^{3+} energy levels still seems to be the most important mechanism of excitation. Whereas the transitions at ~525 and 550 nm de-

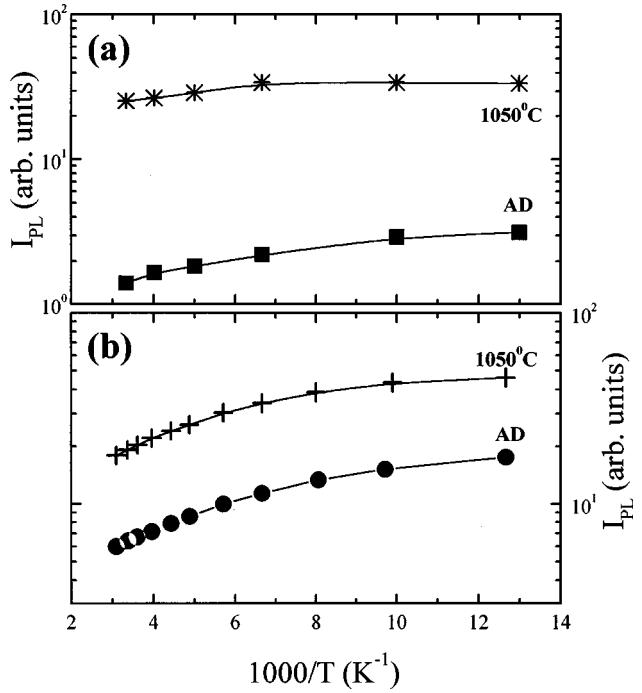

FIG. 8. Photoluminescence intensity (I_{PL}) as a function of the inverse of temperature. (a) I_{PL} sum of the $^2H_{11/2}\rightarrow{}^4I_{15/2}$ and $^4S_{3/2}\rightarrow{}^4I_{15/2}$ transitions. (b) I_{PL} of the $^4I_{13/2}\rightarrow{}^4I_{15/2}$ transition at ~1540 nm observed in sample *D*. AD stands for the as-deposited film, while the curves labeled with 1050 °C were achieved after thermal anneals up to 1050 °C. Note the different dependencies exhibited by VIS and IR radiative transitions as the temperature of measurement is varied.

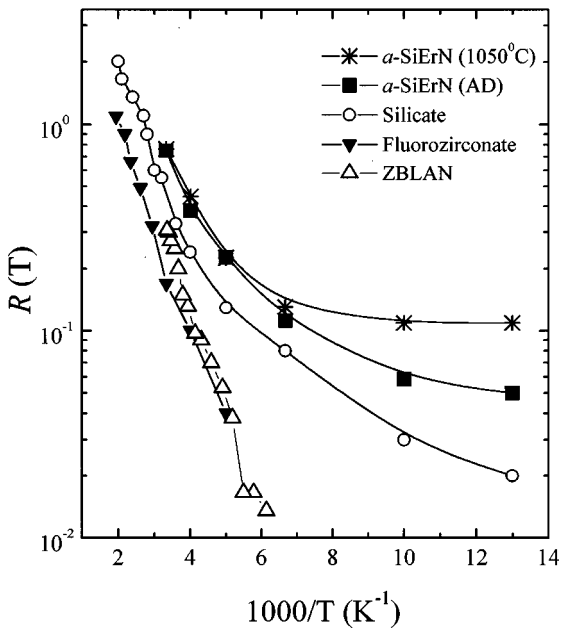

FIG. 9. Photoluminescence intensity ratio $R(T)$ between the $^2H_{11/2}\rightarrow{}^4I_{15/2}$ and $^4S_{3/2}\rightarrow{}^4I_{15/2}$ transitions as a function of inverse temperature. The figure contains data for an as-deposited (AD) *a*-SiErN film and one thermal annealed at 1050 °C. Experimental data from silicate (Ref. 33), fluorozirconate (Ref. 32), and ZBLAN (Ref. 31) glasses were also represented for comparison. ZBLAN is the acronym for (ZrF_4-BaF_2-LaF_3-AlF_3-NaF) glasses. Notice the different activation energies observed near $T\sim250$ K. The lines joining the experimental data are guides to the eyes.

pend mainly on the population of the $^4F_{7/2}$ levels, the emission at ~1540 nm certainly will be subjected to a more complex mechanism (a combination of higher-energy levels and host energy transfer, for example).

In order to explore this behavior in detail, PL as a function of temperature was investigated on the as-deposited and thermal-annealed samples and, as can be seen from Fig. 8, all radiative transitions due to Er^{3+} ions are sensitive to temperature. Since the VIS region contains two different transitions, the values displayed in Fig. 8(a) correspond to the sum of their intensities. Qualitatively, all experimental curves are equivalent: the PL intensities are almost constant at low temperatures, while they experience a great quenching at temperatures higher than ~150 K (as a consequence of nonradiative processes). A fine analysis, however, indicates a stronger temperature dependence of the emission at ~1540 nm [Fig. 8(b)]. In the 300–80 K temperature range, the increase proved by radiative transitions in the IR and in the VIS regions were of ~4 and ~2, respectively. Although that behavior might be fortuitous, it gives support to the idea that the population of the $^2H_{11/2}$ and $^4S_{3/2}$ levels does not depend very much on the energy-transfer processes from the *a* host. Still related to light emission in the VIS region, the $^2H_{11/2}$ energy level is known to be thermally populated from the $^4S_{3/2}$ one.[30,31] This temperature dependence can be expressed by the following ratio $R(T)$ between the PL intensity of the $^2H_{11/2}\rightarrow{}^4I_{15/2}$ and $^4S_{3/2}\rightarrow{}^4I_{15/2}$ transitions:[32]

$$R(T)=\frac{I(^2H_{11/2}\rightarrow{}^4I_{15/2})}{I(^4S_{3/2}\rightarrow{}^4I_{15/2})}=K\exp\left(\frac{-\hbar\omega}{k_BT}\right), \qquad (1)$$

where the constant *K* takes into account the radiative emission probability and the energy-level degeneracy of the two transitions considered. The energy separation between the $^2H_{11/2}$ and $^4S_{3/2}$ levels is denoted by $\hbar\omega$, and k_B is Boltzmann's constant. It is important to notice that the above dependence is only a rough approximation. A more realistic analysis of the population at the $^2H_{11/2}$ energy level should include other possible routes: (non)radiative paths associated with the Er^{3+} ions, optical excitation of the $^2H_{11/2}$ states from higher-energy levels, and energy losses like the tail-to-tail[14,15] PL of the *a*-SiErN host, for example. Figure 9 shows the $R(T)$ of the as-deposited and thermal-annealed sample *D*. The experimental $R(T)$ values of some Er-doped glasses were also represented for comparison.[31–33] As can be seen from Fig. 9, all compounds exhibit a very similar behavior. At temperatures higher than ~250 K the activation energy stays in the 80–110 meV range, indicating a $^2H_{11/2}$-$^4S_{3/2}$ energy level separation of ~800 cm^{-1} (in reasonable agreement with the spectroscopic data).

At lower temperatures ($T\leqslant250$ K), the $R(T)$ ratio clearly points out a smaller activation energy. This weak temperature dependence indicates the existence of at least two different mechanisms related to the population of the $^2H_{11/2}$ level: (i) In view of this small activation energy, and since carrier recombination is always taking place in the *a* host, part of the population of the $^2H_{11/2}$ state originates from matrix—Er^{3+} energy-transfer processes. (ii) All compounds presented in Fig. 9 were optically excited at the $^4F_{7/2}$ (or even higher) energy levels. As a consequence, there should be a nonzero probability of energy transfer from higher-

energy states to the $^2H_{11/2}$ level. The smaller the activation energy at low temperatures (see the *a*-SiErN film treated at 1050 °C in Fig. 9, for example), the smaller will be the dependence of the $^2H_{11/2}$ population on the different phenomena occurring in the *a* host.

V. CONCLUSIONS

Thin films of Er-doped amorphous SiN (*a*-SiErN) alloys have been prepared by cosputtering under different deposition conditions and Er concentrations. Infrared-absorption and Raman-scattering measurements indicate no appreciable differences in both compositional and structural characteristics of these films. Photoluminescence spectroscopy, on the other hand, presented the most remarkable features. According to the experimental results, nonintentionally hydrogenated samples with a large Er content seems to be the best ones for the achievement of very narrow (~20 nm) Er^{3+}-related green light emission. The strongest emissions in the *a*-SiErN films take place at ~525, 550, and 1540 nm, and correspond to transitions from the $^2H_{11/2}$, $^4S_{3/2}$, and $^4I_{13/2}$ levels to the $^4I_{15/2}$ ground state, respectively. The *a*-SIN matrix also exhibits a broad (>100 nm) visible PL signal which stays around 500–600 nm. The present experimental data pointed out the following remarks.

(1) The most convenient way to extract green Er^{3+}-related PL from the *a*-SiErN samples is with 488.0-nm photon excitation, which resonantly populates the $^4F_{7/2}$ energy levels of the Er^{3+} ions.

(2) It is believed that a high number of Er^{3+} ions can improve the optical absorption of 488.0-nm photons which, in association with the absence of hydrogen atoms, partially inhibit the PL due to the *a* matrix.

(3) Isochronal thermal anneals performed on these nonintentionally hydrogenated *a*-SiErN films promote the PL enhancement, at room temperature, of all Er^{3+}-related radiative transitions (at ~1540, 550, and 525 nm), and is closely related to a reduction in the number of nonradiative centers.

(4) PL measurements as a function of temperature indicate the existence of different mechanisms controlling the light emission at ~525–550 nm and at ~1540 nm, the last one being much more sensitive to the host conditions.

(5) The influence of these host conditions can be seen both from the temperature-dependent PL data as well as from the oxygen content in the thermal-annealed samples.

Summarizing, Er^{3+} ions in combination with a wide-band-gap *a*-SiN semiconductor allowed the achievement of very narrow green light emission at room temperature. In addition to the potential applications of SiEr-based compounds in the infrared energy region (light sources, detectors, optical amplifiers, etc.), the present results enlarge the perspectives of their use in the construction of monochromatic large-area flat-panel displays, visible light-emitting diodes, temperature sensors, etc.

ACKNOWLEDGMENTS

This work was partially supported by the Brazilian Agencies FAPESP and CNPq.

[1] See, for example, R. S. Soref, Proc. IEEE **81**, 1687 (1993).
[2] S. S. Iyer and Y. H. Xie, Science **260**, 40 (1993).
[3] L. Brus, J. Phys. Chem. **98**, 3575 (1994).
[4] Y. Kanemitsu, J. Lumin. **70**, 333 (1996).
[5] See, for instance, *Rare-Earth Doped Semiconductors II*, edited by S. Coffa, A. Polman, and R. N. Schwartz, MRS Symposia Preceedings No. 422 (Materials Research Society, Pittsburgh, 1996).
[6] J. W. Fleming, Electron. Lett. **14**, 326 (1978).
[7] J. Palm, F. Gan, B. Zheng, J. Michel and L. Kimerling, Phys. Rev. B **54**, 17 603 (1996).
[8] A. Polman, J. Appl. Phys. **82**, 1 (1997).
[9] A. Kasuya and M. Suezawa, Appl. Phys. Lett. **71**, 2728 (1997).
[10] A. R. Zanatta and L. A. O. Nunes, Appl. Phys. Lett. **72**, 3127 (1998).
[11] F. Priolo, G. Franzò, S. Coffa, and A. Carnera, Phys. Rev. B **57**, 4443 (1998).
[12] G. H. Dieke, *Spectra and Energy Levels of Rare-Earth Ions in Crystals* (Interscience, New York, 1968).
[13] A. J. Steckl and R. Birkhahn, Appl. Phys. Lett. **73**, 1700 (1998).
[14] I. G. Austin, W. A. Jackson, T. M. Searle, P. K. Bhat, and R. A. Gibson, Philos. Mag. B **52**, 271 (1985).
[15] R. A. Street, *Hydrogenated Amorphous Silicon* (Cambridge University Press, Cambridge, 1991).
[16] O. S. Heavens, *Optical Properties of Thin Films* (Dover, New York, 1991).
[17] M. H. Brodsky, M. Cardona, and J. J. Cuomo, Phys. Rev. B **16**, 3556 (1977).
[18] See, for example, A. C. Adams, in *Silicon Nitride and Other Insulator Films, Plasma Deposited Thin Films*, edited by J. Mort and F. Jansen (CRC Press, Boca Raten, FL, 1988), p. 129.
[19] G. Lucovsky and W. B. Pollard, in *Vibrational Properties, The Physics of Hydrogenated Amorphous Silicon II*, edited by J. D. Joannopoulos and G. Lucovsky, Topics in Applied Physics Vol. 56 (Springer-Verlag, Berlin, 1984), p. 301.
[20] K. J. Bachmann, *The Materials Science of Microlectronics* (VCH, New York, 1995), Chap. 6.
[21] N. Wada, S. A. Solin, J. Wong, and S. Prochazka, J. Non-Cryst. Solids **43**, 7 (1981).
[22] P. A. Temple and C. E. Hathaway, Phys. Rev. B **7**, 3685 (1973).
[23] In addition to the relative Er/Si target area, the Er concentration has been determined by means of Rutherford backscattering. Er contents of ~0.5, 1, and 1.5 at. %, correspond to the Er/Si target areas ~0.03, 0.06, and 0.1.
[24] A. R. Zanatta, L. A. O. Nunes, and L. R. Tessler, Appl. Phys. Lett. **70**, 511 (1997).
[25] A. R. Zanatta and L. A. O. Nunes, J. Non-Cryst. Solids **227-230**, 389 (1998).
[26] G. N. van den Hoven, J. H. Shin, A. Polman, S. Lombardo, and S. U. Campisano, J. Appl. Phys. **78**, 2642 (1995).
[27] R. Serna, E. Snoeks, G. N. van den Hoven, and A. Polman, J. Appl. Phys. **75**, 2644 (1994).
[28] A. R. Zanatta and L. A. O. Nunes, Appl. Phys. Lett. **71**, 3679 (1997).
[29] J. Michel, J. L. Benton, R. F. Ferrante, D. C. Jacobson, D. J.

Eaglesham, E. A. Fitzgerald, Y. Xie, J. M. Poate, and L. Kimerling, J. Appl. Phys. **70**, 2672 (1991).
[30] M. A. Chamarro and R. Cases, J. Lumin. **46**, 59 (1990).
[31] T. Yokokawa, H. Inokuma, Y. Ohki, H. Nishikawa, and Y. Hama, J. Appl. Phys. **77**, 4013 (1995).
[32] M. D. Shinn, W. A. Sibley, M. G. Drexhage, and R. N. Brown, Phys. Rev. B **27**, 6635 (1983).
[33] J. A. Capobianco, G. Prevost, P. P. Proulx, P. Kabro, and M. Betinelli, Opt. Mater. **6**, 175 (1996).